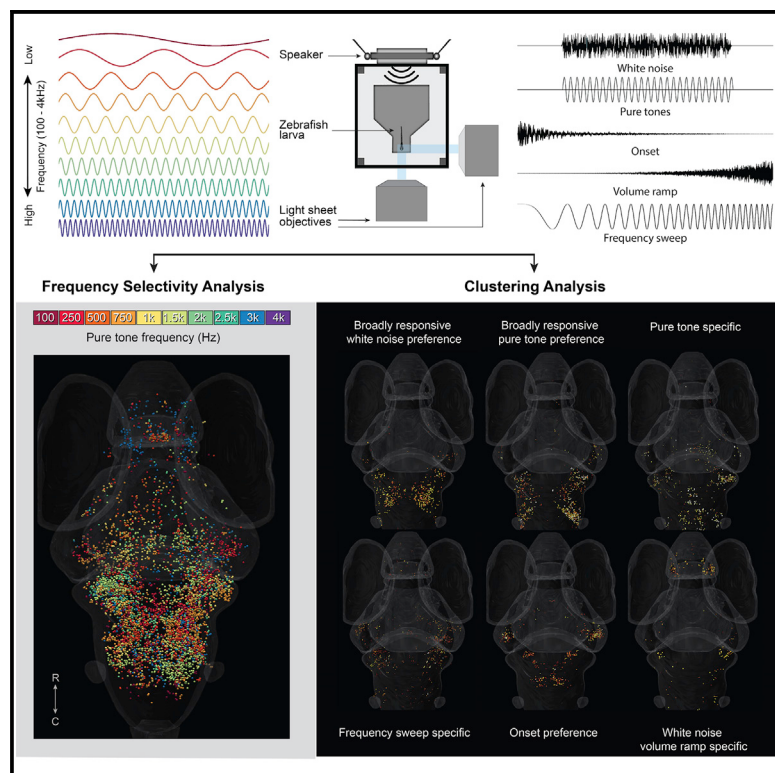


Broad frequency sensitivity and complex neural coding in the larval zebrafish auditory system

Graphical Abstract



Authors

Rebecca E. Poulsen,
Leandro A. Scholz, Lena Constantin,
Itia Favre-Bulle,
Gilles C. Vanwalleghem, Ethan K. Scott

Correspondence

g.vanwalleghem@uq.edu.au (G.C.V.),
ethan.scott@uq.edu.au (E.K.S.)

In brief

Larval fish are thought to have rudimentary auditory systems sensitive to low frequency. Using calcium imaging, Poulsen et al. show neural responses in zebrafish larvae up to 4 kHz, frequency discrimination up to 2.5 kHz, and unique signatures for simple and complex sounds. The particular responses are located in specific locations across the brain.

Highlights

- Larval zebrafish have neural responses to auditory stimuli up to 4 kHz
- Different frequencies elicit distinct responses for frequencies below 2.5 kHz
- Responses distinguish pure versus complex stimuli and gradual versus sharp onset
- Frequency-selective neurons are organized spatially but are not clearly tonotopic



Report

Broad frequency sensitivity and complex neural coding in the larval zebrafish auditory system

Rebecca E. Poulsen,¹ Leandro A. Scholz,¹ Lena Constantin,¹ Itia Favre-Bulle,^{1,2} Gilles C. Vanwalleghem,^{1,*} and Ethan K. Scott^{1,3,4,*}

¹Queensland Brain Institute, The University of Queensland, Brisbane, QLD 4072, Australia

²School of Mathematics and Physics, The University of Queensland, Brisbane, QLD 4072, Australia

³Twitter: @LabEthan

⁴Lead contact

*Correspondence: g.vanwalleghem@uq.edu.au (G.C.V.), ethan.scott@uq.edu.au (E.K.S.)

<https://doi.org/10.1016/j.cub.2021.01.103>

SUMMARY

Most animals have complex auditory systems that identify salient features of the acoustic landscape to direct appropriate responses. In fish, these features include the volume, frequency, complexity, and temporal structure of acoustic stimuli transmitted through water. Larval fish have simple brains compared to adults but swim freely and depend on sophisticated sensory processing for survival.^{1–5} Zebrafish larvae, an important model for studying brain-wide neural networks, have thus far been found to possess a rudimentary auditory system, sensitive to a narrow range of frequencies and without evident sensitivity to acoustic features that are salient and ethologically important to adult fish.^{6,7} Here, we have combined a novel method for delivering water-borne sounds, a diverse assembly of acoustic stimuli, and whole-brain calcium imaging to describe the responses of individual auditory-responsive neurons across the brains of zebrafish larvae. Our results reveal responses to frequencies ranging from 100 Hz to 4 kHz, with evidence of frequency discrimination from 100 Hz to 2.5 kHz. Frequency-selective neurons are located in numerous regions of the brain, and neurons responsive to the same frequency are spatially grouped in some regions. Using functional clustering, we identified categories of neurons that are selective for a single pure-tone frequency, white noise, the sharp onset of acoustic stimuli, and stimuli involving a gradual crescendo. These results suggest a more nuanced auditory system than has previously been described in larval fish and provide insights into how a young animal's auditory system can both function acutely and serve as the scaffold for a more complex adult system.

RESULTS AND DISCUSSION

The auditory systems of fish are crucial for their survival, informing behaviors that include escaping from predators, searching for food, and communicating with each other.^{1–5} There are several properties of sound stimuli that allow fish to extract ethologically important information, including the sounds' frequencies, amplitudes, durations, and whether they are pure tones of a single frequency or complex sounds composed of multiple frequencies. Various fish species have been shown to respond behaviorally to a range of different acoustic stimulus properties,^{2,8–11} and some of the sensory neurons mediating these behaviors have been characterized electrophysiologically.^{12–16} Nonetheless, our understanding of these auditory networks remains incomplete in terms of the categories of responsive neurons, their locations and connections, and the ways in which they work together to process acoustic information.

Zebrafish larvae, which provide unparalleled opportunities for the description of sensory circuits and networks,^{17–20} have thus far been reported to have rudimentary auditory systems.^{6,7} As a result, many of the circuit-level details of complex auditory processing in fish remain unexplored, and it remains unclear whether the larvae of any fish species can discriminate among

the varying complex properties of acoustic stimuli.^{21–23} In this study, we have performed an analysis of larval zebrafish hearing using whole-brain calcium imaging at cellular resolution while applying controlled acoustic stimuli with a range of amplitudes, frequencies, complexities, and durations. Because this approach is both comprehensive (spanning the entire brain) and detailed (resolving individual neurons), it offers the potential to reveal brain-wide auditory networks in a way that has not previously been possible and to shed light on the auditory capabilities that aquatic animals have during the early stages of development.

Our approach required the accurate and reproducible delivery of sound,²⁴ but the air-water interface complicates this stimulation in aquatic systems, especially in cases where underwater speakers are impractical. Past studies have used different approaches for delivering sound to zebrafish larvae,^{9,25–27} and these larvae have variously been shown to respond behaviorally to frequencies up to 200 Hz,^{13,26} 400 Hz,²⁸ or 1,000–1,200 Hz.^{9,25,29} The first calcium imaging study of larval zebrafish hearing, using an air speaker, found strong neural responses in the 100–400 Hz range, with weak responses up to 800 Hz.⁶ A more recent imaging study, using an array of underwater speakers, showed responses from 100 Hz



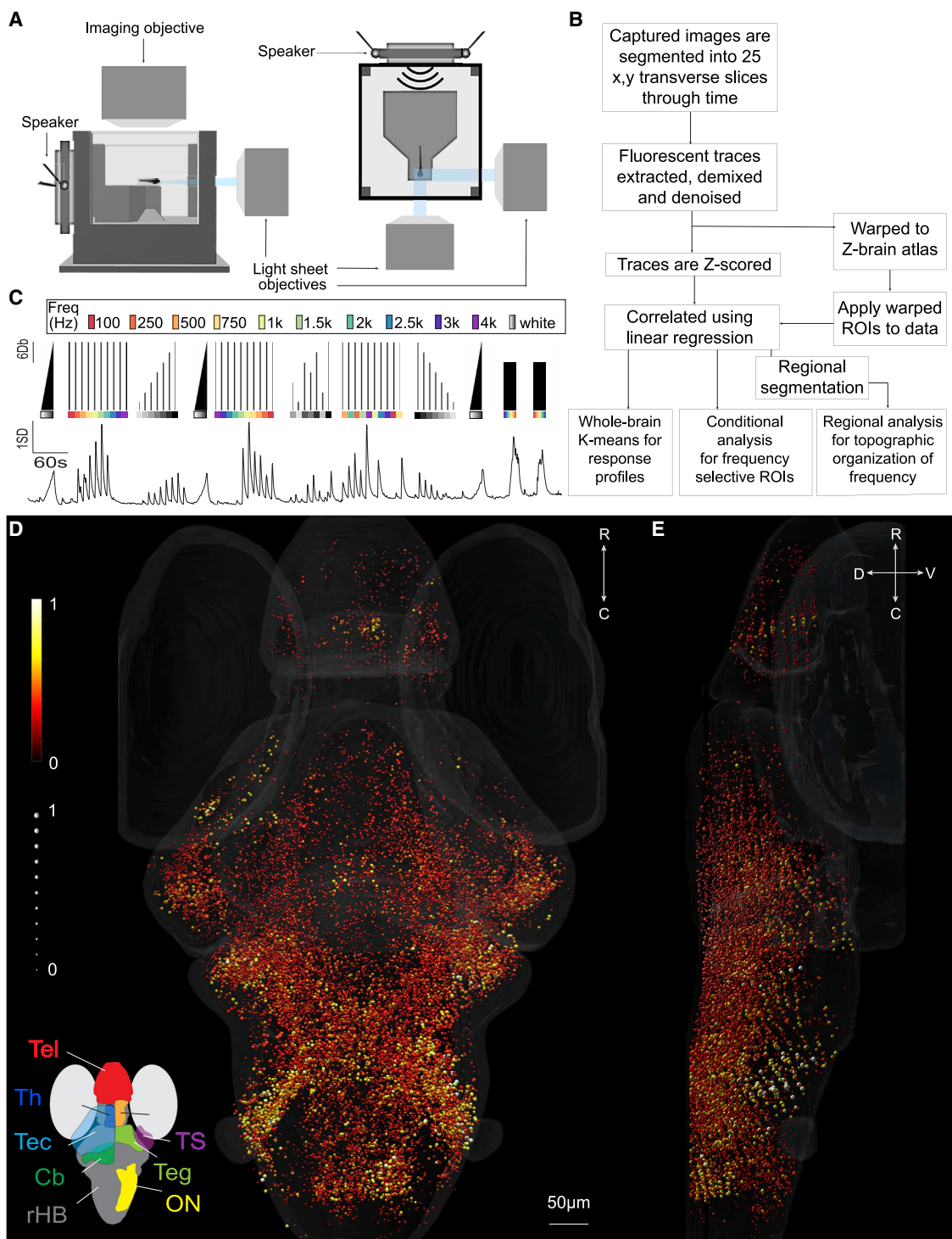


Figure 1. Experimental design, analytic workflow, and auditory-responsive ROIs

(A) Schematic of the imaging and experimental setup used to observe brain activity from zebrafish larvae, showing the mini-speaker attached to the back coverslip of the chamber.

(B) Summary of the analysis workflow used to identify and categorize auditory-responsive neurons across the brain.

(C) Top: a schematic of the stimulus train used, including stimuli with a range of different forms, frequencies, and amplitudes. Bottom: the mean response of all the auditory-responsive ROIs in the resulting dataset is shown.

(D and E) All auditory-responsive ROIs across the brain are shown with the strength of the response represented by the color and the correlation to the linear regression model (r^2 value) represented as the size of the sphere. The strength of the response is between 2 (the threshold for inclusion) and 12 SD. Brain regions containing a high proportion of auditory-responsive ROIs are identified spatially (inset, D).

(legend continued on next page)

to 450 Hz and 950 Hz to 1 kHz, without finding responses to intermediate frequencies.⁷

To avoid the complications that arise from the air-water interface and the interference generated by arrays of speakers, we attached a mini-speaker directly to the back coverslip wall of our 3D printed imaging chamber, effectively turning the coverslip into a water-coupled speaker (Figure 1A). The fidelity of the resulting stimuli was tested with a single-axis accelerometer (to detect particle motion) and a hydrophone (to detect the pressure wave), confirming the power distribution of each frequency (Figure S1; STAR methods). Using this approach, we ensonified the chamber with a diverse set of acoustic stimuli (Figure 1C) that fell into two basic categories: pure tones of individual frequencies ranging from 100 Hz to 4 kHz and white noise stimuli composed of frequencies throughout this range. The pure tones were used to explore frequency selectivity, while white noise stimuli of various amplitudes allowed us to study response sensitivity. With the goal of studying auditory sensitivity rather than escape behavior, we chose a maximum volume that reliably produced strong brain activity without eliciting startle responses (data not shown). In addition to our individual 1-s stimuli, we included 20-s white noise amplitude ramps, with an amplitude increasing from silence to full volume, and frequency sweeps with ascending or descending frequencies between 100 Hz and 4 kHz across a 30-s stimulus.

Auditory responses are widespread across the brain

To observe brain-wide responses to these stimuli, we performed volumetric calcium imaging using dual-plane selective plane illumination microscopy (SPIM) (Figure 1A) and the *HuC:H2B-GCaMP6f* transgenic line.^{30,31} Volumetric images were collected, processed, and analyzed using the neuroinformatic pipeline outlined in Figure 1B (see Vanwallegem et al.⁶ and STAR methods for details). Briefly, we started by segmenting regions of interest (ROIs) generally corresponding to individual neurons and then used linear regression and thresholding to identify all auditory-responsive ROIs (Figure 1B; STAR methods). The mean signal of these collective ROIs showed responses to all stimuli in our stimulus train except for pure tones at high frequencies (Figure 1C). Using the three-dimensional positions of each ROI, registered against the Zbrain atlas of the larval zebrafish brain (Figure 1B; STAR methods),³² we mapped all responsive ROIs onto a reference brain, including the strength (regression coefficient) and correlation coefficient of the auditory responses of each ROI (Figures 1D and 1E).

The resulting map of brain-wide auditory responses revealed ROIs throughout numerous regions of the brain, including all regions that have previously been described as auditory responsive in larval zebrafish.^{6,7,33,34} Auditory responses were particularly dense and strong in the octavolateralis nucleus (ON), which receives direct innervation from both the ears and lateral line^{35,36} and relays this information to other regions of the brain.^{37,38} Our previous work showing that these responses persist after lateral line ablation⁶ and our use of acoustic frequencies that are mostly

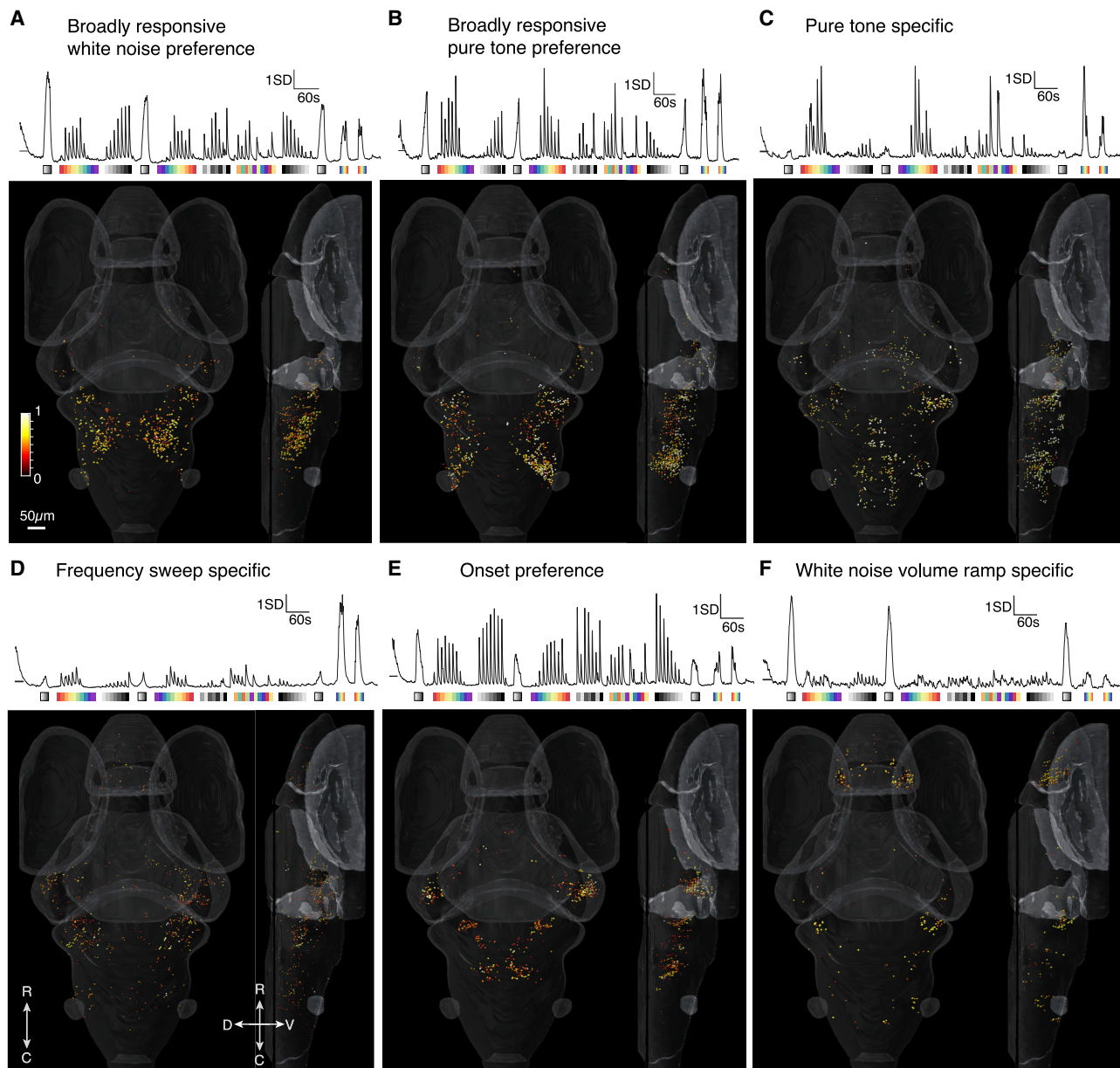
above the lateral line's detection range³⁹ led us to conclude that a vast majority of these ON responses are auditory. Beyond the ON, we observed robust auditory responses in structures including the torus semicircularis (TS), thalamus, cerebellum, and the remaining hindbrain (HB) (excluding the ON and cerebellum). Responses were sparser but nonetheless clear in the tectum, telencephalon, tegmentum, and pretectum, with a small number of auditory ROIs in the habenulae. We also used a supervised approach to detect stimulus-associated drops in the GCaMP signal that are indicative of inhibition (STAR methods)⁴⁰ but found no consistent evidence of auditory-responsive neurons that were inhibited.

Evidence of selective responses to complex acoustic features

Although these results reveal the locations of auditory neurons across the brain, they do not demonstrate whether different categories of neurons, with selective responses to particular stimuli, exist within this system. To explore this possibility, we performed k-means clustering (STAR methods) to identify functional categories (clusters) of ROIs responding to individual sound properties or categories of properties. Using this approach, we found a total of six clusters of ROIs with distinct response types. Two of these clusters were broadly tuned, responding to all of the stimuli except for the highest frequency pure tones (Figures 2A and 2B). The first of these (Figure 2A) showed its strongest responses to white noise stimuli, including those at a low amplitude. The second broadly tuned cluster (Figure 2B) was less sensitive to white noise stimuli but showed stronger responses to pure tones across a range of frequencies. Interestingly, ROIs belonging to these clusters were restricted to the ON and, to a much lesser degree, the TS. Given that the ON, which is homologous to the cochlear nucleus in mammals, is the first brain structure to receive information from the ear, this suggests that the early stage of auditory processing in larval zebrafish involves broadly tuned neurons, consistent with findings from other fish species.^{36,38} However, as these clusters' preferences for white noise or pure tones were not absolute, it is possible that there is a range of broadly responsive ROIs in the ON and that these two clusters represent two halves of a diverse continuum of such neurons.

A third functional cluster included ROIs that responded almost exclusively to pure tones across a range of frequencies (Figure 2C). These ROIs were distributed across the ON, TS, HB, and tegmentum. This distribution closely resembles that of the fourth cluster (found in the ON, TS, tectum, and remaining HB and sparsely in the thalamus and telencephalon; Figure 2D), in which the ROIs were specifically responsive to frequency sweeps. These clusters have responses to pure tones in common, whether those tones occurred in isolation (Figure 2C) or at different times during a frequency sweep (Figure 2D), suggesting that the auditory-responsive ROIs in these regions are involved in the detection of pure tones and potentially the discrimination of different frequencies.

Cb, cerebellum; HB, remaining hindbrain; ON, octavolateralis nucleus; Tec, tectum; Teg, tegmentum; Tel, telencephalon; Th, thalamus; TS, torus semicircularis. C, caudal; D, dorsal; R, rostral; V, ventral here and in subsequent figures. Scale bar applies to both (D) and (E). Particle motion and sound pressure recordings of the chamber can be found in Figure S1.

**Figure 2. K-means clustering of brain-wide auditory-responsive ROIs**

K-means clustering revealed 6 clusters of ROIs that respond to particular properties of acoustic stimuli.

(A and B) Two broadly tuned clusters were detected that were predominately located in the ON.

(C) A pure-tone-specific cluster was present in the medial HB, lateral cerebellum, TS, and pretectum.

(D) A third cluster, selective for pure tones, was detected with ROIs in the TS, ON, and lateral cerebellum.

(E) An onset cluster was present in the TS, the lateral cerebellum, and the medial HB.

(F) The final cluster revealed white noise volume ramp-selective ROIs located in the pallial region of the telencephalon, the lateral cerebellum, and sparsely in the HB.

Scale bar applies to all panels. Response strengths and r^2 values are represented as in Figure 1.

A fifth cluster contained ROIs that responded strongly to stimuli with sudden onsets (square tones), including both pure tones and white noise stimuli and stimuli with very low amplitudes. In contrast, they had relatively weak responses to acoustic volume ramps, even once these ramps reached their peak amplitudes (Figure 2E). We interpret these to be “onset” ROIs that are specifically sensitive to the sudden occurrence of sound. These

ROIs were particularly abundant in the TS and were also present in the ON and, to a lesser degree, the thalamus. This cluster indicates that the larval zebrafish TS is particularly sensitive to the onset of a sound, spanning from the lowest frequency played (100 Hz), through to 3 kHz, and to all white noise volumes. A reciprocal cluster (Figure 2F) responded almost exclusively to white noise ramp stimuli, with little or no response to stimuli

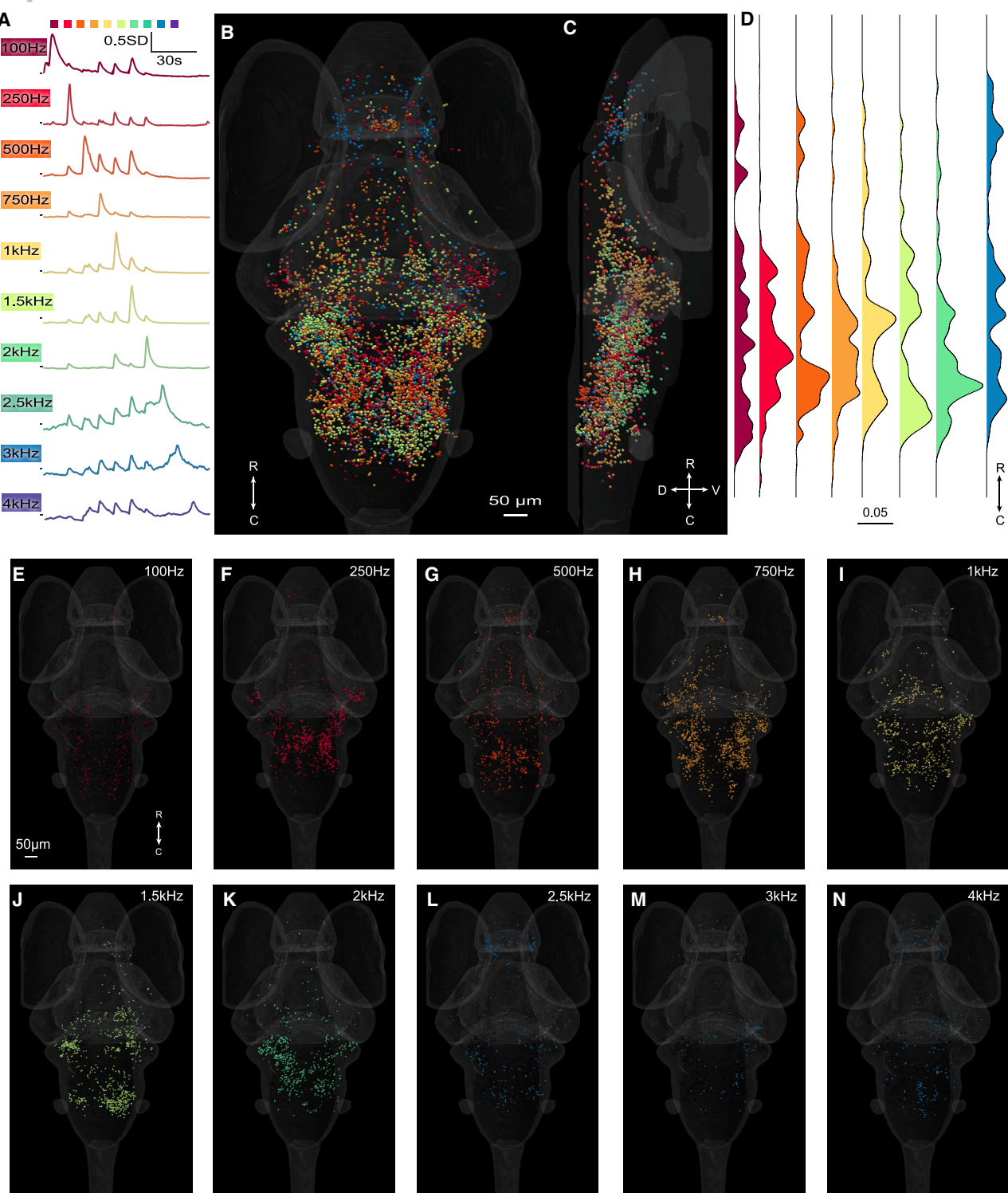


Figure 3. Frequency specificity and homogeneity at the whole-brain level

(A–C) The mean responses (A) of all ROIs selectively responding to each frequency in our stimulus train (top) and (B) their positions in the brain from a dorsal view and (C) a lateral view. Scale bar applies to both (B) and (C).

(D) Using a one-dimensional kernel density estimation (KDE) computation, we looked at the density of frequency-selective ROIs at the whole-brain level, from rostral to caudal. Because of the overlapping responses and similar spatial distributions of ROIs responding to 2.5-kHz, 3-kHz, and 4-kHz tones, we combined these into a single category for (C) and (D).

(legend continued on next page)

with sharp onsets. This cluster's distribution was distinct from those of the other five clusters, with ROIs predominantly restricted to the lateral pallium and lateral cerebellum. Taken together, these findings indicate that larval zebrafish have neurons selective to a range of specific properties of sound by 6 dpf.

The application of a clustering approach with our brain-wide imaging data provides a framework for understanding more nuanced auditory processing than has previously been described in any larval fish species. The identification of these diverse and specialized auditory neurons, with selective responses to pure versus complex tones and to the onset of square tones versus ramps, suggests that some of the sophistication of the adult fish auditory system^{3,24,36,37,41,42} is already in place in zebrafish larvae at 6 dpf. The larval brain is anatomically much simpler than that of adults and lacks nucleation of key auditory structures, including the ON and thalamus. Nonetheless, there are hints in our results that the overall architecture of the adult pathway is present, in a nascent form, in these larvae. This complexity at the larval stage could both underpin the discrimination of distinct acoustic events by larval fish and could also provide a framework for incorporating more-nuanced auditory signals through development, especially with the subsequent development of the Weberian ossicles.^{5,25}

Evidence for frequency discrimination across the 100 Hz–2.5 kHz range

Adult zebrafish have been shown to discriminate different frequencies in behavioral experiments,⁴³ but it is less clear whether such discrimination takes place in larval fish (zebrafish or otherwise). Our previous work has suggested that there is little or no frequency discrimination among ON neurons in larval zebrafish,⁶ although a recent study from Privat et al.⁷ proposed distinct neural pathways for broad bands of high- and low-frequency sounds at the whole-brain level. Overall, the larval zebrafish literature suggests a detection range up to roughly 1 kHz, with, at best, coarse frequency discrimination across this range.^{9,25,29} Having identified a large population of ROIs across the brain that respond to pure tones (Figure 2), we next explored whether their responses provide evidence for frequency discrimination or the topographic representation of different frequencies across or within brain regions.³⁷

To conduct this analysis, we adopted a supervised approach, building regressors for each frequency of pure tone in our stimulus train and applying regressions to the auditory responsive ROIs (Figures 1D and 1E). We then defined an ROI as frequency selective if its regression coefficient (response strength) was greater than 2.5 SD above the mean distribution for that frequency, and below 2.0 SD for all other frequencies (STAR methods). Applying these criteria to 35,720 auditory ROIs across seven larvae, we identified 9,411 ROIs that qualified as frequency selective (Figure 3A). The average traces of neurons selective to each frequency peaked much higher (>2-fold) than adjacent frequencies through the low-mid frequency range (up to 2 kHz; Figure 3A). In contrast, those for 2.5 kHz, 3.0 kHz,

and 4.0 kHz-responsive ROIs were similar to the adjacent frequencies (Figure 3A). This suggests that larval zebrafish may be sensitive to these higher 2.5–4 kHz frequencies without being able to discriminate among them, although discrimination among lower frequencies seems likely. We next mapped the locations of frequency-selective ROIs throughout the brain (Figures 3B and 3C). Although we found most of the ROIs spanned the rostro-caudal extent of the brain, we did not see whole-brain tonotopy, with the most frequency-selective ROIs located in the hindbrain, including the ON. This was especially true for ROIs that were selective to the mid frequencies (750–2,000 Hz). The low (100 Hz) and high (2.5–4.0 kHz) frequencies were more broadly dispersed along the rostro-caudal axis, including notable concentrations of ROIs in the telencephalon (Figure 3D). For frequencies above 2.5 kHz, these responses tended to involve the lateral telencephalon, where ROIs responsive to lower frequencies were concentrated in the medial telencephalon (Figure 3B).

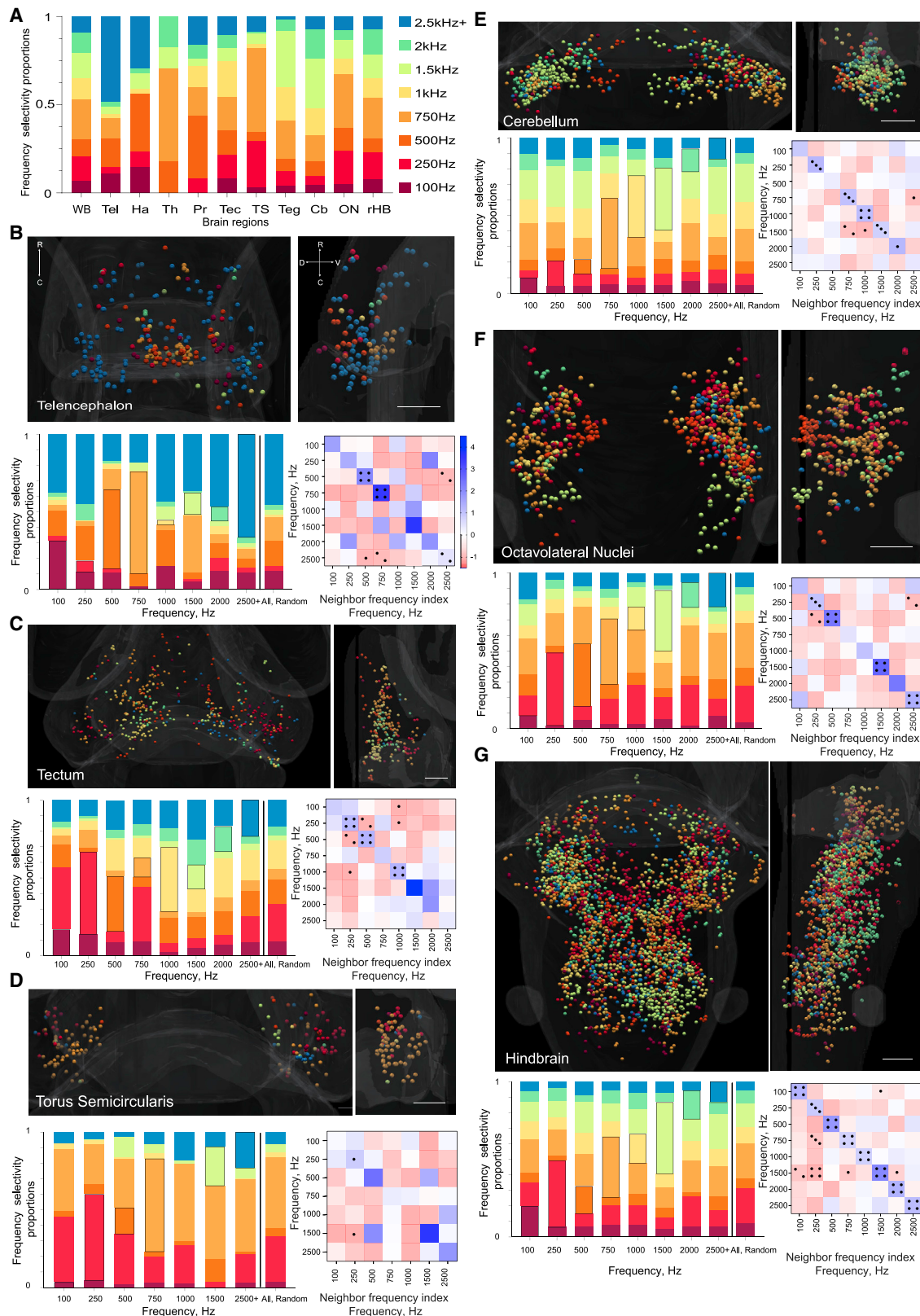
These results depend on the fidelity and specificity of our delivered acoustic stimuli, and these can be complicated in small chambers like ours. Because we saw pronounced harmonics at higher frequencies during our 100-Hz stimulation (Figure S1), it is possible that the breadth of responses at this frequency are, in fact, the products of off-target stimulation. In all trials, we detected a weak low-frequency signal using our accelerometer, although not using our hydrophone (Figure S1). This arose either from noise in the accelerometer or detection system itself or potentially from a low-frequency hum from our speaker. This off-target signal is well below the detection limit of our larvae according to our exploration of sensitivity in Figure 1. It is also present in all trials, including control trials without directed acoustic stimuli. This demonstrates that responses in other trials are, indeed, the products of the targeted acoustic stimulation.

A recent study by Privat et al.⁷ showed two regions of frequency sensitivity, ranging from 150 to 450 Hz and 950 Hz to 1 kHz (the highest frequency tested), which were represented primarily in the hindbrain and midbrain, respectively. In this prior study, no responses were observed to frequencies between these ranges. Their use of geometric ROIs presumed to encompass numerous neurons could explain the absence of intermediate frequencies from their study, consistent with the fact that we often found our 500-Hz- and 750-Hz-responsive neurons intercalated with ROIs responding to other frequencies. Furthermore, they used a cytoplasmically targeted GCaMP, providing the benefit that they could analyze responses in neuropil regions (which our nuclear-targeted GCaMP did not reveal) but at the cost of resolving individual neurons. Finally, their study targeted particular parts of the brain for imaging and may therefore have missed responses that we have found in regions not previously associated with auditory processing in this system.

Spatial grouping of frequency-selective ROIs

In mammals and some adult fish, auditory responses are organized tonotopically, whereby the frequency specificities of the

(E–N) Dorsal views showing ROIs of each frequency used in the stimulus train that passed the supervised analysis thresholding. The relevant frequency is indicated in each panel. Although the sound level to both ears is equal, there is asymmetry in the ROIs passing threshold due to the fish being illuminated from the front and one side. The right side, which receives a brighter and sharper SPIM plane, generally yields more ROIs that pass our inclusion criteria.



(legend on next page)

neurons correlate with their spatial positions.^{37,42,44–46} Although such tonotopy is not required for the discrimination of different frequencies, it would nonetheless be interesting in phylogenetic and ontogenetic terms if it were present in larval zebrafish. In larval zebrafish, a previous study from our group has hinted at tonotopy, albeit inconclusively,⁶ whereas Privat et al.⁷ have suggested broad brain-wide segregation of high- and low-frequency responses without responses to intermediate frequencies. To search for topographical encoding of frequency in our dataset, we carried out a spatial analysis of frequency-selective ROIs in ten brain regions that were prominent in our brain-wide dataset or that are known to be involved in auditory processing.^{6,7,33,34,38} These regions were the ON, TS, thalamus, pretectum, tectum, habenula, tegmentum, telencephalon, cerebellum, and remaining HB. Collectively, these regions include 97% of frequency-responsive ROIs in our dataset. Because of the overlapping responses and similar spatial distributions of ROIs responding to 2.5 kHz, 3.0 kHz, and 4.0 kHz tones (Figure 3), we combined these into a single category for this analysis.

The broad frequency tuning of each brain region can be gauged by comparing the abundance of the frequency selectivities of its ROIs to those of ROIs across the entire brain (Figure 4A). The most striking departures from brain-wide averages were found in the telencephalon and to a lesser degree in the TS, both of which were enriched for responses to high frequencies (Figure 3B). The telencephalon was notable for its segregation of high- and low-frequency ROIs. Low-frequency responses are abundant in the medial telencephalon, which is homologous to the amygdala in mammals,^{47,48} whereas high-frequency responses are concentrated in the lateral telencephalon, which corresponds to the mammalian hippocampus.^{49,50} The thalamus was minimally responsive to high and low frequencies, responding instead to frequencies from 500 Hz to 2 kHz. Other brain regions exhibited frequency-responsive ROIs whose relative proportions approximately reflected those across the brain as a whole.

To search for frequency-related topography in each of these brain regions, we next performed a k-nearest neighbor (kNN) analysis, whereby, for each ROI selective to a given frequency, we observed a selected number (k) of nearest neighbors and recorded the frequency selectivity of those neighbors (STAR methods). The results of this nearest neighbor analysis were then compared to a randomized dataset where the same number of ROIs of each frequency were retained, but the frequency selectivities of these ROIs were reassigned randomly. We performed 100 iterations of this randomization and compared the neighbors yielded from these random datasets to those seen in our actual imaging dataset (Figure 4). The rationale for this

approach was that heterogeneous distributions of frequency-selective neurons, where neurons responding to a particular frequency are spatially clustered, should result in a higher prevalence of same-frequency neighbors in our experimental dataset versus the randomized datasets.

Each brain region had its own profile of frequency-responsive ROIs (Figure 4A), and in each brain region, the randomized nearest neighbor population closely reflected this overall abundance of each frequency (Figures 4B–4H, “all random” bar; k neighbors listed in STAR methods). We could identify spatial clustering of the ROIs of each frequency by looking for cases where the same frequency was overrepresented among its neighbors (dark boxes in each bar), as compared to neighbors from the “all randomized” bar. To quantify these effects, we generated a “neighbor frequency index” (STAR methods). This gives positive values (shown in blue, Figures 4B–4G) when a given frequency is overrepresented among the neighbors and negative values (red) when that frequency is underrepresented. Accordingly, spatial clustering of ROIs with the same frequency sensitivity should be represented by positive values along the diagonal of each matrix (bottom right, Figures 4B–4G), and tonotopy would drive positive values in squares adjacent to the diagonal.

Using our kNN analysis, we found numerous cases in which same-frequency ROIs were spatially clustered (Figures 4B–4G). The distributions of ROIs in the primary auditory region, the ON (Figure 4F), appeared to have the lower frequencies spatially organized in the dorsomedial section, with the populations representing the higher frequencies being located more caudally and the low frequencies more rostrally. In most regions, there were examples of significantly elevated neighbor frequency indices for ROIs responding to the same frequency (blue diagonal lines, Figures 4B–4G), with these being particularly prominent in the tectum, cerebellum, ON, and hindbrain, where all same-frequency indices were elevated, many of them significantly. This was not consistently the case in the TS, where the very high abundance of 250-Hz- and 750-Hz-responsive ROIs may have limited the sensitivity of the frequency neighbor index. In the thalamus, the pretectum, and the habenulae, there were not enough ROIs to support a statistical analysis of their spatial distribution (these distributions are shown in Figure S3). In the tegmentum, there were no statistically significant departures from a homogeneous distribution of ROIs responding to different frequencies, suggesting a lack of spatial frequency representation (Figure S3).

Although our nearest neighbor analysis identified numerous examples of spatially clustered same-frequency ROIs, it provided scant evidence for tonotopy. The distributions of

Figure 4. Regional frequency distribution and tonotopy

(A) The fraction of ROIs per frequency at the whole-brain (WB) and regional levels. Remaining brain regions now shown here can be found in Figure S2. (B–G) The spatial distribution of ROIs from the dorsal (top left) and lateral (top right) views are shown. Bar graphs (bottom left) show the proportions of nearest neighbors for ROIs of a given frequency preference (separate bars for ROIs responding to different frequencies), with same-frequency neighbors indicated by a black box. For comparison, data from the spatially randomized dataset are shown in the last bar. Matrices (bottom right) of the neighbor frequency index show pairs of frequencies that are overrepresented (blue, bar in B) or underrepresented (red) as neighbors. Significant results versus the randomized dataset are indicated ($\cdot p < 0.05$; $\cdot\cdot p < 0.01$; $\cdot\cdot\cdot p < 0.001$; $\cdot\cdot\cdot\cdot p < 0.0001$). See Figure S3 for p values. Kruskal-Wallis tests with Dunn’s correction for multiple comparisons were performed to establish p values. The k-nearest neighbor heatmap legend is shown in (B) and applies to (B)–(G). The same information for the remaining brain regions can be found in Figure S2, and all p values are presented in Figure S3. Figure S4 shows additional whole-brain responses to logarithmic frequencies from 251 to 1,998 Hz at the original volume and 3 lower volumes, –6, –12, and –18 dB below. Scale bars represent 50 μ m.

ROIs in the primary auditory region, the ON (Figure 4F), appeared to have the lower frequencies spatially organized in the dorso-medial section, with the populations representing the higher frequencies being located more caudally. The tectum (Figure 4C) also appeared to contain a medial (high frequency) to lateral (low frequency) gradient, while the HB (Figures 3D and 4G) appeared to have a rostral (low frequency) to caudal (middle frequency) gradient. None of these trends, however, was confirmed by consistently elevated frequency neighbor indices for consecutive frequencies, which would have appeared as significantly blue cells adjacent to the diagonals in Figure 4.

In other animal models, high-amplitude acoustic stimuli can lead to a blurring of frequency selectivity, potentially obscuring tonotopy that might be present at lower volumes.^{51,52} To test whether more-pronounced tonotopy might be present at lower volumes, we performed an additional experiment in which 10 frequencies were presented at 6, 12, or 18 dB below our standard amplitude (**STAR methods**). These analyses showed no refinement of topography at the lower volumes (Figure S4). This suggests that the level of spatial grouping and the absence of pronounced tonotopy reported in Figures 3 and 4 is representative of the best spatial segregation to be found in 6-dpf zebrafish larvae.

Overall, the observations from our nearest neighbor analysis suggest that, although neurons responding to a given frequency are spatially clustered at multiple stages of the auditory processing pathway in larval zebrafish, systematic tonotopy is absent or still in a rudimentary form. Details of our approach and statistical tests mean that these represent conservative interpretations. We observed several cases where strong positive neighbor frequency index scores proved to be non-significant. These generally occurred where the brain region as a whole (the TS, for instance) or the frequency being tested (1.5 kHz in the tectum, for example) had a small number of ROIs. It is likely that larger datasets would reveal significance in these relationships, as they did in the HB (Figure 4G), where a large number of ROIs show significance in all same-frequency comparisons. We also note that our cases of strong same-frequency clustering may be masking tonotopy, given that a high abundance of same-frequency ROIs in a neighbor pool depletes the pool for other frequencies, including adjacent ones. This may provide a partial explanation for the lack of significant tonotopy in our analyses, although it is also possible that this tonotopy simply does not exist in zebrafish larvae, only emerging in later stages of development in teleosts.^{37,42,53–55}

Summary and conclusions

Previous studies have described the auditory sensitivity and hearing range of larval zebrafish using a range of different approaches,^{5–7,9,25} generally describing a system with limited sensitivity to stimulus components, a tight frequency range, and little spatial specialization in auditory coding. In this study, we have used a more diverse stimulus train, a novel method for sound delivery, and an upgraded imaging system to detect and characterize the brain-wide responses of individual neurons in larval zebrafish. We have revealed response characteristics that suggest broad auditory tuning in the early stages of the network, especially in the ON, and sensitivity to more-nuanced stimulus properties in later stages, including in the TS,

telencephalon, cerebellum, and remaining HB. These later steps may provide sensitivity to pure tones, the detection of the onset of acoustic stimuli, and the detection of stimuli that ascend in intensity gradually.

We have also shown broader frequency sensitivity, up to 4 kHz, than has previously been observed and spatial clustering of frequency-selective neurons in several brain regions, although this is not reflected in coherent patterns of tonotopy. The potential for frequency discrimination appears to be restricted to frequencies below 2.5 kHz, as frequencies from 2.5 to 4.0 kHz elicit indistinguishable patterns of neural activity. Furthermore, at higher frequencies, response strengths are not strongly linked to stimulus amplitude (Figure S4). As such, although zebrafish larvae appear to detect frequencies as high as 4 kHz, nuances like frequency discrimination and amplitude sensitivity may only occur at lower frequencies.

Nonetheless, these results suggest a broader range of frequency responses than are expected for larval fish, raising the question of the mechanism by which this detection occurs. One possibility is that frequency selectivity arises in the peripheral auditory system as seen in adult goldfish,⁴² perhaps through the activity of frequency-specific hair cells,^{37,42,56} and identifying the mechanisms by which signals from the ear already carry frequency information represents a clear goal for future work in this system. The detection of higher frequencies could also be mediated by pressure sensitivity, which would depend on compression of the swim bladder. This capability is thought to depend on the development of the Weberian apparatus, which is absent at the larval stage in zebrafish. One possibility, though, is that passive vibration of the otoliths by expansion and compression of the swim bladder could provide sensitivity to higher frequencies. In the future, this possibility could be addressed by manipulations of the swim bladder^{57–59} or bio-optical-acoustic vibrations of the otoliths.⁶⁰ In total, our results provide evidence for more-sophisticated auditory processing than has previously been appreciated in larval zebrafish and offers a departure point for characterizing the physical mechanisms, the local circuits, and the brain-wide networks that mediate this sensory processing.

STAR★METHODS

Detailed methods are provided in the online version of this paper and include the following:

- **KEY RESOURCES TABLE**
- **RESOURCE AVAILABILITY**
 - Lead contact
 - Materials availability
 - Data and code availability
- **EXPERIMENTAL MODEL AND SUBJECT DETAILS**
 - Animals
- **METHOD DETAILS**
 - Calcium imaging
 - Acoustic stimulation
- **QUANTIFICATION AND STATISTICAL ANALYSIS**
 - Data processing and analysis
 - Data visualization
 - Statistical analysis

SUPPLEMENTAL INFORMATION

Supplemental Information can be found online at <https://doi.org/10.1016/j.cub.2021.01.103>.

ACKNOWLEDGMENTS

We thank the University of Queensland's Biological Resources aquatics team for animal care. We also thank Emmanuel Marquez-Legorreta for his intellectual expertise regarding telencephalic activity. We thank Germán Sumbre and Rowan Tweedale for suggestions on the manuscript. Support was provided by NHMRC project grants APP1066887 and APP1165173, a Simons Foundation Pilot Award (399432), a Simons Foundation Research Award (625793), and two ARC Discovery Project Grants (DP140102036 and DP110103612) to E.K.S. and the Australian National Fabrication Facility (ANFF), QLD node. The research reported in this publication was supported by the National Institute of Neurological Disorders and Stroke of the National Institutes of Health under award number R01NS118406 to E.K.S. The content is solely the responsibility of the authors and does not necessarily represent the official views of the National Institutes of Health. G.C.V. was supported by an EMBO Long-term Fellowship, and R.E.P. and L.S. were supported by University of Queensland Postgraduate Awards.

AUTHOR CONTRIBUTIONS

Conceptualization, E.K.S. and R.E.P.; Methodology, R.E.P., G.C.V., I.F.-B., and L.S.; Investigation, R.E.P. and G.C.V.; Animal Colony Maintenance, L.C.; Formal Analysis, R.E.P., G.C.V., and L.S.; Data Curation, R.E.P. and G.C.V.; Writing – Original Draft, R.E.P. and E.K.S.; Writing – Review & Editing, G.C.V., R.E.P., L.S., L.C., and I.F.-B.; Figure Construction, R.E.P. and L.S.; Funding Acquisition, E.K.S.; Resources, E.K.S.; Supervision, E.K.S. and L.C.

DECLARATION OF INTERESTS

The authors declare no competing interests.

Received: September 23, 2020

Revised: December 16, 2020

Accepted: January 28, 2021

Published: March 2, 2021

REFERENCES

1. Eaton, R.C., and Didomenico, R. (1986). Role of the teleost escape response during development. *Trans. Am. Fish. Soc.* **115**, 128–142.
2. Fay, R.R., and Simmons, A.M. (1999). The sense of hearing in fishes and amphibians. In *Comparative Hearing: Fish and Amphibians*, R.R. Fay, and A.N. Popper, eds. (Springer New York), pp. 269–318.
3. McKibben, J.R., and Bass, A.H. (1999). Peripheral encoding of behaviorally relevant acoustic signals in a vocal fish: single tones. *J. Comp. Physiol. A Neuroethol. Sens. Neural Behav. Physiol.* **184**, 563–576.
4. McKibben, J.R., and Bass, A.H. (2001). Peripheral encoding of behaviorally relevant acoustic signals in a vocal fish: harmonic and beat stimuli. *J. Comp. Physiol. A Neuroethol. Sens. Neural Behav. Physiol.* **187**, 271–285.
5. Higgs, D.M., Rollo, A.K., Souza, M.J., and Popper, A.N. (2003). Development of form and function in peripheral auditory structures of the zebrafish (*Danio rerio*). *J. Acoust. Soc. Am.* **113**, 1145–1154.
6. Vanwalleghem, G., Heap, L.A., and Scott, E.K. (2017). A profile of auditory-responsive neurons in the larval zebrafish brain. *J. Comp. Neurol.* **525**, 3031–3043.
7. Privat, M., Romano, S.A., Pietri, T., Jouary, A., Boulanger-Weill, J., Elbaz, N., Duchemin, A., Soares, D., and Sumbre, G. (2019). Sensorimotor transformations in the zebrafish auditory system. *Curr. Biol.* **29**, 4010–4023.e4.
8. Alderks, P.W., and Sisneros, J.A. (2013). Development of the acoustically evoked behavioral response in larval plainfin midshipman fish, *Porichthys notatus*. *PLoS ONE* **8**, e82182.
9. Bhandiwad, A.A., Zeddes, D.G., Raible, D.W., Rubel, E.W., and Sisneros, J.A. (2013). Auditory sensitivity of larval zebrafish (*Danio rerio*) measured using a behavioral prepulse inhibition assay. *J. Exp. Biol.* **216**, 3504–3513.
10. Fay, R.R. (1992). Analytic listening by the goldfish. *Hear. Res.* **59**, 101–107.
11. Yang, Q., Sun, P., Chen, S., Li, H., and Chen, F. (2017). Behavioral methods for the functional assessment of hair cells in zebrafish. *Front. Med.* **11**, 178–190.
12. Eaton, R.C., Lavender, W.A., and Wieland, C.M. (1981). Identification of Mauthner-initiated response patterns in goldfish - evidence from simultaneous cinematography and electrophysiology. *J. Comp. Physiol.* **144**, 521–531.
13. Lu, Z., and DeSmidt, A.A. (2013). Early development of hearing in zebrafish. *J. Assoc. Res. Otolaryngol.* **14**, 509–521.
14. Maruska, K.P., and Sisneros, J.A. (2016). Comparison of electrophysiological auditory measures in fishes. *Adv. Exp. Med. Biol.* **877**, 227–254.
15. Sisneros, J.A., and Bass, A.H. (2005). Ontogenetic changes in the response properties of individual, primary auditory afferents in the vocal plainfin midshipman fish *Porichthys notatus* Girard. *J. Exp. Biol.* **208**, 3121–3131.
16. Wright, K.J., Higgs, D.M., Cato, D.H., and Leis, J.M. (2010). Auditory sensitivity in settlement-stage larvae of coral reef fishes. *Coral Reefs* **29**, 235–243.
17. Simmich, J., Staykov, E., and Scott, E. (2012). Zebrafish as an appealing model for optogenetic studies. *Prog. Brain Res.* **196**, 145–162.
18. Vanwalleghem, G.C., Ahrens, M.B., and Scott, E.K. (2018). Integrative whole-brain neuroscience in larval zebrafish. *Curr. Opin. Neurobiol.* **50**, 136–145.
19. Favre-Bulle, I.A., Vanwalleghem, G., Taylor, M.A., Rubinstein-Dunlop, H., and Scott, E.K. (2018). Cellular-resolution imaging of vestibular processing across the larval zebrafish brain. *Curr. Biol.* **28**, 3711–3722.e3.
20. Marquez-Legorreta, E., Constantin, L., Piber, M., Favre-Bulle, I.A., Taylor, M.A., Vanwalleghem, G.C., and Scott, E. (2019). Brain-wide visual habituation networks in wild type and *fmr1* zebrafish. *bioRxiv*. <https://doi.org/10.1101/722074>.
21. Bass, A.H., and McKibben, J.R. (2003). Neural mechanisms and behaviors for acoustic communication in teleost fish. *Prog. Neurobiol.* **69**, 1–26.
22. Maruska, K.P., and Tricas, T.C. (2009). Encoding properties of auditory neurons in the brain of a soniferous damselfish: response to simple tones and complex conspecific signals. *J. Comp. Physiol. A Neuroethol. Sens. Neural Behav. Physiol.* **195**, 1071–1088.
23. Wysocki, L.E., and Ladich, F. (2003). The representation of conspecific sounds in the auditory brainstem of teleost fishes. *J. Exp. Biol.* **206**, 2229–2240.
24. Popper, A.N., Hawkins, A.D., Sand, O., and Sisneros, J.A. (2019). Examining the hearing abilities of fishes. *J. Acoust. Soc. Am.* **146**, 948.
25. Zeddes, D.G., and Fay, R.R. (2005). Development of the acoustically evoked behavioral response in zebrafish to pure tones. *J. Exp. Biol.* **208**, 1363–1372.
26. Higgs, D.M., Souza, M.J., Wilkins, H.R., Presson, J.C., and Popper, A.N. (2002). Age- and size-related changes in the inner ear and hearing ability of the adult zebrafish (*Danio rerio*). *J. Assoc. Res. Otolaryngol.* **3**, 174–184.
27. Thompson, A.W., Vanwalleghem, G.C., Heap, L.A., and Scott, E.K. (2016). Functional profiles of visual-, auditory-, and water flow-responsive neurons in the zebrafish tectum. *Curr. Biol.* **26**, 743–754.
28. Bang, P.I., Yelick, P.C., Malicki, J.J., and Sewell, W.F. (2002). High-throughput behavioral screening method for detecting auditory response defects in zebrafish. *J. Neurosci. Methods* **118**, 177–187.
29. Burgess, H.A., and Granato, M. (2007). Sensorimotor gating in larval zebrafish. *J. Neurosci.* **27**, 4984–4994.

30. Chen, T.W., Wardill, T.J., Sun, Y., Pulver, S.R., Renninger, S.L., Baohan, A., Schreiter, E.R., Kerr, R.A., Orger, M.B., Jayaraman, V., et al. (2013). Ultrasensitive fluorescent proteins for imaging neuronal activity. *Nature* **499**, 295–300.
31. Taylor, M.A., Vanwalleghem, G.C., Favre-Bulle, I.A., and Scott, E.K. (2018). Diffuse light-sheet microscopy for stripe-free calcium imaging of neural populations. *J. Biophotonics* **11**, e201800088.
32. Randlett, O., Wee, C.L., Naumann, E.A., Nnaemeka, O., Schoppik, D., Fitzgerald, J.E., Portugues, R., Lacoste, A.M., Riegler, C., Engert, F., and Schier, A.F. (2015). Whole-brain activity mapping onto a zebrafish brain atlas. *Nat. Methods* **12**, 1039–1046.
33. Bae, Y.K., Kani, S., Shimizu, T., Tanabe, K., Nojima, H., Kimura, Y., Higashijima, S., and Hibi, M. (2009). Anatomy of zebrafish cerebellum and screen for mutations affecting its development. *Dev. Biol.* **330**, 406–426.
34. Constantin, L., Poulsen, R.E., Scholz, L.A., Favre-Bulle, I.A., Taylor, M.A., Sun, B., Goodhill, G.J., Vanwalleghem, G.C., and Scott, E.K. (2020). Altered brain-wide auditory networks in a zebrafish model of fragile X syndrome. *BMC Biol.* **18**, 125.
35. Liao, J.C., and Haehnel, M. (2012). Physiology of afferent neurons in larval zebrafish provides a functional framework for lateral line somatotopy. *J. Neurophysiol.* **107**, 2615–2623.
36. Tomchik, S.M., and Lu, Z. (2006). Auditory physiology and anatomy of octavolateral efferent neurons in a teleost fish. *J. Comp. Physiol. A Neuroethol. Sens. Neural Behav. Physiol.* **192**, 51–67.
37. Echteler, S.M. (1985). Organization of central auditory pathways in a teleost fish, *Cyprinus carpio*. *J. Comp. Physiol. A* **156**, 267–280.
38. Edds-Walton, P.L., and Fay, R.R. (2008). Directional and frequency response characteristics in the descending octaval nucleus of the toadfish (*Opsanus tau*). *J. Comp. Physiol. A Neuroethol. Sens. Neural Behav. Physiol.* **194**, 1013–1029.
39. Levi, R., Akanyeti, O., Ballo, A., and Liao, J.C. (2015). Frequency response properties of primary afferent neurons in the posterior lateral line system of larval zebrafish. *J. Neurophysiol.* **113**, 657–668.
40. Vanwalleghem, G., Constantin, L., and Scott, E.K. (2021). Calcium imaging and the curse of negativity. *Front. Neural Circuits* **14**, 607391.
41. Fay, R.R. (1995). Perception of spectrally and temporally complex sounds by the goldfish (*Carassius auratus*). *Hear. Res.* **89**, 146–154.
42. Smith, M.E., Schuck, J.B., Gilley, R.R., and Rogers, B.D. (2011). Structural and functional effects of acoustic exposure in goldfish: evidence for tonotopy in the teleost saccule. *BMC Neurosci.* **12**, 19.
43. Cervi, A.L., Poling, K.R., and Higgs, D.M. (2012). Behavioral measure of frequency detection and discrimination in the zebrafish, *Danio rerio*. *Zebrafish* **9**, 1–7.
44. Mann, Z.F., and Kelley, M.W. (2011). Development of tonotopy in the auditory periphery. *Hear. Res.* **276**, 2–15.
45. Hackett, T.A., Barkat, T.R., O'Brien, B.M., Hensch, T.K., and Polley, D.B. (2011). Linking topography to tonotopy in the mouse auditory thalamocortical circuit. *J. Neurosci.* **31**, 2983–2995.
46. Humphries, C., Liebenthal, E., and Binder, J.R. (2010). Tonotopic organization of human auditory cortex. *Neuroimage* **50**, 1202–1211.
47. Maximino, C., Lima, M.G., Oliveira, K.R., Batista, Ede.J., and Herculano, A.M. (2013). “Limbic associative” and “autonomic” amygdala in teleosts: a review of the evidence. *J. Chem. Neuroanat.* **48-49**, 1–13.
48. von Trotha, J.W., Vernier, P., and Bally-Cuif, L. (2014). Emotions and motivated behavior converge on an amygdala-like structure in the zebrafish. *Eur. J. Neurosci.* **40**, 3302–3315.
49. Ganz, J., Kroehne, V., Freudenreich, D., Machate, A., Geffarth, M., Braasch, I., Kaslin, J., and Brand, M. (2014). Subdivisions of the adult zebrafish pallium based on molecular marker analysis. *F1000Res.* **3**, 308.
50. Mueller, T., Dong, Z., Berberoglu, M.A., and Guo, S. (2011). The dorsal pallium in zebrafish, *Danio rerio* (Cyprinidae, Teleostei). *Brain Res.* **1381**, 95–105.
51. Guo, W., Chambers, A.R., Darrow, K.N., Hancock, K.E., Shinn-Cunningham, B.G., and Polley, D.B. (2012). Robustness of cortical topography across fields, laminae, anesthetic states, and neurophysiological signal types. *J. Neurosci.* **32**, 9159–9172.
52. Bowen, Z., Winkowski, D.E., and Kanold, P.O. (2020). Functional organization of mouse primary auditory cortex in adult C57BL/6 and F1 (CBAxC57) mice. *Sci. Rep.* **10**, 10905.
53. Andersen, R.A., and Enger, P.S. (1968). Microphonic potentials from the sacculus of a teleost fish. *Comp. Biochem. Physiol.* **27**, 879–881.
54. Wubbels, R.J., and Schellart, N.A. (1998). An analysis of the relationship between the response characteristics and topography of directional- and non-directional auditory neurons in the torus semicircularis of the rainbow trout. *J. Exp. Biol.* **201**, 1947–1958.
55. Echteler, S.M. (1985). Tonotopic organization in the midbrain of a teleost fish. *Brain Res.* **338**, 387–391.
56. Rogers, L.S., and Sisneros, J.A. (2020). Auditory evoked potentials of utricular hair cells in the plainfin midshipman, *Porichthys notatus*. *J. Exp. Biol.* **223**, jeb226464.
57. Ehrlich, D.E., and Schoppik, D. (2017). Control of movement initiation underlies the development of balance. *Curr. Biol.* **27**, 334–344.
58. Goolish, E.M., Okutake, K., and Johnson, P. (2000). The behavioral response of zebrafish to hypergravity conditions. *J. Gravit. Physiol.* **7**, 99–100.
59. Friedmann, B.R., and Shutty, K.M. (1999). Effect of timing of oil film removal and first feeding on swim bladder inflation success among intensively cultured striped bass larvae. *N. Am. J. Aquaculture* **61**, 43–46.
60. Favre-Bulle, I.A., Taylor, M.A., Marquez-Legorreta, E., Vanwalleghem, G., Poulsen, R.E., Rubinsztein-Dunlop, H., et al. (2020). Sound generation in zebrafish with Bio-Opto-Acoustics (BOA). *Nat. Comm.* **11**, 6120.
61. Panier, T., Romano, S.A., Olive, R., Pietri, T., Sumbre, G., Candelier, R., and Debrégeas, G. (2013). Fast functional imaging of multiple brain regions in intact zebrafish larvae using selective plane illumination microscopy. *Front. Neural Circuits* **7**, 65.
62. Edelstein, A., Amodaj, N., Hoover, K., Vale, R., and Stuurman, N. (2010). Computer control of microscopes using μ Manager. *Curr. Protoc. Mol. Biol. Chapter 14*, Unit14.20.
63. Pnevmatikakis, E.A., and Giovannucci, A. (2017). NoRMCorre: an online algorithm for piecewise rigid motion correction of calcium imaging data. *J. Neurosci. Methods* **291**, 83–94.
64. Avants, B.B., Epstein, C.L., Grossman, M., and Gee, J.C. (2008). Symmetric diffeomorphic image registration with cross-correlation: evaluating automated labeling of elderly and neurodegenerative brain. *Med. Image Anal.* **12**, 26–41.
65. Vanwalleghem, G., Schuster, K., Taylor, M.A., Favre-Bulle, I.A., and Scott, E.K. (2020). Brain-wide mapping of water flow perception in zebrafish. *J. Neurosci.* **40**, 4130–4144.

STAR★METHODS

KEY RESOURCES TABLE

REAGENT or RESOURCE	SOURCE	IDENTIFIER
Deposited data		
Imaging data	ESpace	https://doi.org/10.14264/680dfce
Statistical analysis	Github	https://github.com/Scott-Lab-QBI/Brainwide_auditory_processing
Experimental models: organisms/strains		
Tupfel long fin Nacre	Zirc	ZDB-GENO-080307-1
Tg(elavl3:H2B-GCaMP6f)	³⁰	ZDB-TGCONSTRCT-150916-4
Software and algorithms		
ImageJ	Fiji	https://imagej.nih.gov/ij/
Advanced Normalization Tools	Github	https://github.com/ANTsX/ANTs
MATLAB	Mathworks	https://www.mathworks.com/products/matlab.html (RRID: SCR_001622)
Unity	Unity Technologies	https://unity.com/
Live!	Ableton	https://www.ableton.com/en/live/
Illustrator	Adobe	https://www.adobe.com/au/products/illustrator.html
SPAN	Voxengo	https://www.voxengo.com/product/span/
Python 3.6	N/A	https://www.python.org/ (RRID: SCR_008394)
numpy	N/A	https://doi.org/10.1038/s41586-020-2649-2 (RRID: SCR_008633)
scikit-learn	N/A	https://dl.acm.org/doi/10.5555/1953048.2078195
pandas	N/A	https://doi.org/10.5281/zenodo.3509134 (RRID: SCR_018214)
matplotlib	N/A	https://doi.org/10.5281/zenodo.4030140 (RRID: SCR_008624)
scipy	N/A	https://doi.org/10.1038/s41592-019-0686-2 (RRID: SCR_008058)

RESOURCE AVAILABILITY

Lead contact

Further information and requests for resources should be directed to and will be fulfilled by the Lead Contact, Associate Professor Ethan Scott (e.scott@uq.edu.au).

Materials availability

This study did not generate new unique reagents.

Data and code availability

The dataset generated and analyzed for this study can be found in the UQ eSpace <https://doi.org/10.14264/680dfce>, and the code used in the analysis can be found at https://github.com/Scott-Lab-QBI/Brainwide_auditory_processing.

EXPERIMENTAL MODEL AND SUBJECT DETAILS

Animals

Adult zebrafish (*Danio rerio*) were maintained at 28.5°C at a density of 10–15 fish per liter and on a 14/10 hour light/dark cycle. The *HuC:H2B-Gcamp6f* transgenic line was used for these experiments, targeting the calcium indicator GCaMP6f to the nuclei of all neurons.³⁰ Fertilized eggs of the TLN strain were transferred into E3 medium (distilled water with 10% Hanks solution, consisting of 137 mM NaCl, 5.4 mM KCl, 0.25 mM Na₂HPO₄, 0.44 mM KH₂PO₄, 1.3 mM CaCl₂, 1.0 mM 654 MgSO₄ and 4.2 mM NaHCO₃ at pH 7.2) and kept at 28.5°C in an incubator with a 14/10 hour light/dark cycle. Zebrafish housing, breeding, larval maintenance, and experiments were performed with approval from the University of Queensland Animal Ethics Committee (IMB/237/16/BREED and SBS/341/19).

METHOD DETAILS

Calcium imaging

6dpf larval zebrafish were set in a 2% low melting point agarose (Progen Biosciences), dorsal side up, and placed it into the custom-made chamber.³⁴ The 3D printed 24x24mm chamber consists of a square plastic base and a 0.2 mm² post in each corner. 20 mm x

20mm glass coverslips (ProSciTech) were fixed on to each side using a waterproof glue (Liquid Fusion Clear Urethane Adhesive). The glass coverslips enabled light-sheet illumination from the front and one side of the animal with minimal light distortions. Acoustic stimuli were delivered from the speaker adhered to the rear coverslip. Agarose-set fish were mounted onto the platform of the chamber with additional agarose to prevent the fish from moving throughout the experiment. Once the agarose had set, the chamber was filled with E3 medium and allowed to sit for a minimum of 30 minutes to minimize drifting of the fish during imaging.

Whole-brain calcium fluorescence imaging was done using a custom-built selective plane illumination microscope (SPIM) to determine the neural responses *in vivo* while the acoustic stimuli were presented.^{31,61} The fish was simultaneously illuminated with two planes from the front and one side and imaged at 10 μ m increments in the dorsoventral axis with an exposure time of 10ms. This produced a 25-slice volumetric representation of the entire brain, with a 4 Hz volumetric imaging rate. Details of this microscope and imaging procedure have been described previously.^{19,31}

Acoustic stimulation

Acoustic stimulation was provided by a mini speaker (Dayton Audio DAEX-9-4SM Skinny Mini Exciter Audio, Haptic Item Number 295-256) fixed to the back-glass surface (caudal to the animal) of the imaging chamber and wired to an amplifier (Dayton Audio DA30 2 × 15W Class D Bridgeable Mini Amplifier). The speaker was attached to the back wall using 3M VHB adhesive to provide even sound presentation to both ears of the fish. Testing was done to determine the optimal speaker capabilities. Because larval zebrafish have previously been shown to detect particle motion, but perhaps not the pressure wave component of sound,²⁵ we measured the sound pressure and the particle motion for the frequencies used. To measure the particle acceleration within the chamber, we used an accelerometer (PCB Piezotronics, Q353B34) with a sensitivity of 98.7 mV/g. The side-to-side (x axis) and the front-back (y axis) motions were recorded by adhering the accelerometer to the side or front glass coverslip of the chamber, respectively. Vertical particle motion (Z axis) was recorded by suspending the accelerometer (wrapped in a thin latex membrane) above the fish's position in the liquid media. The signal was acquired using National Instruments Signal Express, a vibration input module (NI-9234), and a DAQ (cDAQ-9171). The accelerometer was sensitive to frequencies up to 2000 Hz. We continued the recording using the highest sample rate while playing the frequencies higher than 2kHz, to see if there were subharmonics at this frequency, which would then show up on the spectrogram. Three chambers were tested, and each chamber was tested three times. The data were recorded with MATLAB and analyzed using pspectrum to determine the power distributions of each frequency. These analyses showed that there are no sub-harmonic frequency resonances below the fundamental tone at any of the frequencies tested. There is some higher harmonics in the 100Hz tone which may be due to the speaker's capabilities. With all other frequencies, the strongest harmonic was at least 25dB below the fundamental, which would be close or below the hearing sensitivity of the fish.³⁴

To test the sound pressure component of our stimuli, a custom-built hydrophone (Neptune Sonar, UK) was used to take spectral analysis recordings of the white noise and individual frequencies while the chamber contained E3 medium, and without the fish present. The recording was done by placing the microphone in the water-filled chamber. This was then connected to an Edirol FA-66 microphone preamplifier audio interface (Roland, Japan) and recorded into a professional audio program (Ableton Live!, Germany). The spectral analysis was performed using a Fast Fourier Transform plugin SPAN (Voxengo, Sweden) and showed the white noise response at lower frequencies attenuating at 150 Hz, and high frequencies beginning to attenuate at 6 kHz. The recordings also delineated one of the limitations of the speaker delivery system design. There was a comparably low frequency response at 100Hz in the white noise and individual frequency recordings. The individual pure tones contained minimal harmonic distortion. The response at 100 Hz also contained upper harmonic frequencies, although these had lower amplitudes than the fundamental. The frequency showing the most secondary harmonics was 250 Hz. This was approximately 21 dB below the fundamental, meaning that the fundamental was over three times the amplitude of any harmonic across all frequencies, which was at or below the hearing threshold of the fish.³⁴ Secondary harmonics for other frequencies were all more than 40 dB below the fundamental. During the experiments, the chamber was fastened to the platform to minimize any sonic or motion artifacts that might have resulted from vibrations.

Stimulus playback and image acquisition were performed using Micro Manager software.^{19,62} Each presentation of the primary stimulus train included a 20 s white noise amplitude ramp, 1 s of 10 frequencies with a 2 ms rise and fall time (100, 250, 500, 750, 1000, 1500, 2000, 2500, 3000, 4000 Hz) at 0 dBFS (decibels digital Full Scale) with 9 s inter-stimulus intervals (ISIs), and one second white noise with a 2 ms rise and fall time at 7 amplitudes ranging from -18 dBFS to 0 dBFS in 3 dB increments with a 9 s ISI. This train was presented 3 times, changing the order of the type of stimulus, and using ascending, descending and quasi-random orders of frequencies, and ascending, quasi-random and descending orders of amplitudes. There was 30 s rest between each stimulus type and stimulus presentation.

For the supplemental dataset, in which we looked at frequency selectivity at multiple volumes, images were obtained in the same way as the primary dataset, using 25 slices at two frames per second. The stimulus train consisted of 10 frequencies: 251, 316, 289, 501, 630, 794, 1000, 1258, 1584, and 199 5Hz. These frequencies were chosen based on the previous results of the primary experiment, logarithmically distributed, with the goal of more evenly distributing frequencies across the relevant range. Each frequency is played once at the original volume, and -6, -12 and -18dB below the highest volume, and stimuli were presented with 14 s inter-stimulus intervals. Data were collected for 10 6dpf fish. Accelerometer readings of the frequencies used in this experiment were performed in the Z axis to ensure there were not any harmonics in the new frequencies (Figure S4).

QUANTIFICATION AND STATISTICAL ANALYSIS

Data processing and analysis

We excluded three fish because the imaging quality was poor or the fish were tilted. Of the remaining ten fish, once the images were captured, videos were cropped, the transverse slices were segmented to identify ROIs corresponding to individual neurons, and the data were resaved as 25 individual Z stacks per experiment over time, using ImageJ v1.52c. Each of the 25 planes was then motion corrected using the NoRMCorre algorithm.⁶³ Fluorescent traces generated by calcium transients in each ROI were then extracted, demixed, and denoised using the CalmAn package previously described.^{6,19,63} These traces were then z-scored, and correlated using linear regression, which was built from the stimulus train.

MATLAB v9.5 (Mathworks) was used to further analyze the data. Linear regression was used to extract the auditory-responsive ROIs, and a regressor was built for each of the stimulus types: white noise ramps, individual pure tone sine waves, short white noise volumes, and frequency sweeps. This gives an indication of baseline and stimulus-driven activity and identified neurons that respond to the stimulus train. The motion-corrected 3D volumes were registered, using Advanced Normalization Tools (ANTs, <https://github.com/ANTsX/ANTs>), to the H2B-RFP reference of Zbrain.^{32,64} The resulting warps were then applied to the centroid positions of the ROIs, which allowed us to use their location within brain regions outlined by Zbrain to conduct region-specific analysis.⁶⁵ Three additional fish did not successfully warp to Zbrain and were excluded at this point, leaving an n = 7.

Response types to the properties of sound were then categorized at a brain-wide level. We looked at the correlation coefficient of the fluorescence traces to each acoustic stimulus type (10 pure tones, white noise volumes, frequency sweep for both increasing and decreasing frequency order), thresholding at an r^2 value of 0.1 and a regressor coefficient (response strength) threshold of 2.0 SD above the mean response. K-means clustering was then used as part of the analysis to look at brain-wide profile response types. Given that k-means forces every ROI into a cluster, we used an additional filter of an r^2 value of 0.5, when compared to the mean of that cluster to further clean up the data and remove ROIs that did not match the cluster. The analysis returned 15 clusters. From this, 3 non-auditory-responsive clusters, 4 clusters that were under-represented in more than half the fish, and 2 noisy clusters were excluded, leaving the 6 clusters shown in Figure 3.

To look for frequency heterogeneity, a supervised conditional analysis was conducted to determine whether any of the ROIs were responsive to an individual frequency. For an ROI to be characterized as being frequency specific, its response must be 2.5SD above the mean response strength for that particular frequency and its response must be less than 2.0 SD above the mean response strength at all other frequencies. We looked at responses at thresholds from 1.0 SD to 3.0 SD and determined that 2.5 SD provided the most accurate representation of the data, as 1.0 SD left too many noisy responses, and 3.0 SD left very few ROIs passing threshold. We first looked at this across the brain and subsequently in all the auditory regions to determine if there were whole-brain⁷ or regional⁶ spatial representations of frequency. Regionally, we looked at areas previously indicated to be responsive to sensory processing, namely, the ON, TS, thalamus, telencephalon, cerebellum, tectum, tegmentum, habenula and HB. We also used the inverse criteria to look for potential ROIs whose response would be inhibited at a specific frequency (response had to be 2.5SD below the mean response strength to a particular frequency), but identified no inhibited ROIs.⁴⁰

To look specifically for potential inhibited responses, which would appear as negative deviations, we used a similar approach as above, but using responses 2.5 SD less than the mean response for a specific frequency. We could not locate any consistent inhibited responses (shared across fish) which would fit those criteria.

Data visualization

To give a visual representation of the data, clusters were mapped back onto the brain using Unity which has been adapted into a data visualization system. An isosurface mesh of the zebrafish brain was generated from the Zbrain masks for the diencephalon, mesencephalon, rhombencephalon, telencephalon and eyes using ImageVis3D.^{19,20} The mesh was imported in Unity and overlaid to the ROIs. Each ROI was represented as a sphere within the brain. This enabled a 3D visualization of the resulting clusters and provided a qualitative way to determine if there were any spatially significant results.

Statistical analysis

To quantify spatial frequency heterogeneity at a brain-wide and regional level, a multi-dimensional density estimation was done to determine how the individual frequencies were arranged spatially at a whole-brain level (Figure 3D). This calculated the density of each frequency on the rostro-caudal axis. In order to characterize whether the frequency-selective ROIs showed any kind of spatial segregation, a kNN analysis was carried out. This was done brain-wide and regionally. All code related to these computations is available in https://github.com/Scott-Lab-QBI/Brainwide_auditory_processing.

The spatial position of each group of frequency-selective ROIs was used as input to a 1D (Figure 3D) kernel density estimation (KDE) computation. The sklearn.neighbors.KernelDensity method from python's scikit-learn module was used for this purpose. To compute the KDE, a Gaussian kernel was used and the optimal bandwidth was found through optimization of the log probability density under the KDE model with the sklearn.model_selection.GridSearchCV method. The range of bandwidth values was chosen to ensure that it covered three orders of magnitude up to a third of the maximum range of values in the dimension where the KDE was computed (e.g., if values in the rostro-caudal axis had a range of 1000 pixels, the range of bandwidths tested was from 3 to 300 pixels). For the brain-wide density plots in Figure 3D, the bandwidth was defined as a weighted average of the optimal bandwidths found for each frequency.

The characterization of topographic organization of frequency-selective ROIs of the primary dataset was performed through the kNN analysis. The kNN classifier receives a set of data points (the xyz coordinates of the ROIs in this case) and labels (the frequency for which the ROI is selective) and a parameter k and outputs a decision boundary in the xyz space that defines the most likely label for an ROI with those particular coordinates based on the labels of its k neighbors. In cases where a brain region contained a sufficient number of ROIs for each frequency (minimum of 4) in the right lateral area, only the ROIs that side were used. However, in two of the regions, the telencephalon and tegmentum, the ROIs located in the left lateral area were translated to be merged to the other area based on the detected midline (coordinate origin value of the medial-lateral axis, $y = 315$ pixels), with the merged set of points being used as the input.

The `sklearn.neighbors.KNeighborsClassifier` method was used together with `sklearn.model_selection.cross_val_score` in order to evaluate the accuracy of the classifier for values of k ranging from 1 to 100. Once the accuracy values were obtained, a k value was chosen so that it was not lower than 10 or higher than 20% of the total number of ROIs in that region. This means that we did not necessarily choose the k values that resulted in the highest accuracy but used the results to guide our choice of k to calculate the fraction of neighbors for each frequency (stacked bar graphs in [Figure 4](#)). The K chosen for each brain region was cerebellum: 20, hindbrain: 27, tectum: 13, ON: 19, TS: 11, telencephalon: 12, tegmentum: 27.

In order to quantify how spatially segregated the frequency-selective ROIs in each brain region were, a new set of ROIs was generated. The number of labels for each frequency was kept the same as for the raw data, but they were reassigned to different xyz coordinates using a uniform random distribution. The neighbors were then computed using the same k used in the real dataset. This was performed multiple times for each frequency with a different number of ROIs with new random label assignments (10, 50 and a maximum of 100 iterations). This analysis allowed us to identify how different the spatial distributions of the ROIs were when compared to the same set of xyz coordinates, but with frequency labels assigned randomly in space. The stacked bar graphs in [Figures 4B–4G](#) show the mean of the neighbor fractions with all frequencies considered (e.g., the value of 100 Hz neighbors in telencephalon is the mean 100Hz neighbor fraction of the ROIs of all frequencies). This was done because the mean and standard deviation of the neighbor fractions across frequencies did not change with frequency. The heatmaps show the ratio of the difference between the fraction of neighbors of each frequency in the raw data and the ROIs with randomized frequency labels which we defined as the neighboring frequency index (NFI). The NFI is obtained by $NFI = (n_{real,freq} - n_{random,freq}) / n_{random,freq}$, where $n_{real,freq}$ is the neighbor fraction of the experimental data for a certain frequency and $n_{real,random}$ the neighbor fraction of the same frequency in a dataset containing the same numbers of frequency-responsive neurons of each type, but randomly reassigned to the ROIs in the dataset. The statistical analyses were done to compare the distribution of neighbor fractions of each ROI in the raw data per frequency and per brain region (n available in [Figure S3G](#)) against the neighbor fractions of the 100 ROIs with random reassigned labels per frequency and brain region. We used the non-parametric Kruskal-Wallis test with Dunn's correction for multiple comparisons to obtain the adjusted p values.

Analysis for the supplemental dataset was done by extracting the auditory responsive ROIs using a linear regression with a single regressor per frequency, and a single regressor for the intensities of all the frequencies. Because the distribution of r^2 was higher than the previous dataset, an additional filter of 0.2 was applied (where the r^2 value had to be greater than 0.2). We then calculated the maximum response of each ROI passing this threshold to the 4 amplitudes of the 10 frequencies presented, resulting in a number of neurons \times 40 matrix. The matrices were then clustered per fish, with 20 clusters, resulting in one 20×40 matrix for each fish. In each matrix, we selected the 10 clusters that represented the best response to each frequency we sorted the rows of the 20×40 matrices along the 1st, then 2nd, 3rd, and 4th intensity for that specific frequency. This gave us one 10×40 matrix for each fish, which we averaged across all fish.